A Theoretical Study of the Bifurcation Reaction of Formic Acid: Dynamics around the Intrinsic Reaction Coordinate

Osamu TAKAHASHI, Kuniharu ITOH, Akio KAWANO and Ko SAITO*

Department of Chemistry, Graduate School of Science, Hiroshima University, 1-3-1, Kagamiyama, Higashi-Hiroshima 739-8526, JPN

Abstract

Transition state structures, activation energies, and the intrinsic reaction coordinate(IRC) for the two decomposition paths of formic acid are studied using Hartree-Fock and density functional theory. Formic acid decomposes via the following competing paths; to (1) H_2O + CO and to (2) H_2 + CO_2. Experimental results which were obtained by Saito et al. have shown that the rate constant of path (2) is smaller than that of path (1) by about forty times over the experimental temperature range. On the other hand, calculated results using high level ab initio calculations such as MP4/cc-pVQZ//B3LYP/cc-pVTZ show that the activation energies of paths (1) and (2) are comparable. Detailed examinations of the mode coupling between the vibrational modes and the IRC's suggest that the large difference in the rate constants between

the two reaction paths is attributable to the difference in curvature of the potential energy surfaces for the reaction paths around the IRC.

key word: formic acid, thermal decomposition, bifurcation reaction, IRC, reaction-path Hamiltonian

1 Introduction

There have been reported many experimental [1–6] and theoretical [5,7–10] investigations on the thermal decomposition of formic acid in the gas phase. It is well-known that formic acid has two dissociation paths in the homogeneous gas phase: one is to form CO, the other is to form CO_2.

$$\mathrm{HCOOH} \longrightarrow \mathrm{H_2O + CO} \quad (1)$$

$$\longrightarrow \mathrm{H_2 + CO_2}. \quad (2)$$

Saito et al. [5] have studied these reactions in Ar using the shock tube over the temperature range of 1370-2000 K. They monitored the IR emission intensities at 3.4 and 4.6 μm, corresponding to the reactant of CH stretching and carbon monoxide of vibration, respectively. They determined the second order rate constants as $k_{1,0}=10^{14.32}\exp(\text{-}40.4 \text{ kcal mol}^{-1}/RT)$ and $k_{2,0}=10^{15.13}\exp(\text{-}60.6 \text{ kcal mol}^{-1}/RT)$ in units of $\mathrm{cm^3 mol^{-1} s^{-1}}$, respectively. Contrary to the results of Hsu et al. [4], $k_{2,0}$ values are smaller than $k_{1,0}$ by about two orders, being consistent with the other experiments [1–3] and also their ab initio molecular orbital(MO) calculations. However, their MO calculations were not of sufficient accuracy for quantitative consideration.

Recent progress in quantum chemistry has made it possible to calculate a reliable potential energy surface to describe a chemical reaction. Recently, as an another reaction mechanism for formic acid, bimolecular with H_2O catalysed reaction mechanism for the thermal decomposition using a modified Gaussian 2(G2M) method was reported by Tokmakov et al. [10]. In this case, potential barrier heights corre-

sponding to the above reactions are comparable. However, as in the present case at temperatures above 1500K, the dissociation is mainly a unimolecular process, and the catalysed reactions are neglected in the shock tube experiment. Thus, we need more detailed information for the potential energy surfaces about the two decomposition paths of formic acid.

It is popular to calculate the intrinsic reaction coordinate(IRC) [11] for understanding the reaction path, which is defined as the steepest descent path in mass-weighted Cartesian coordinates. Detailed information is available from the vibrational analysis around the IRC's. These analyses for the decomposition of formic acid have been reported by Yamashita et al. [12]. However, since their early work was performed using the Hartree-Fock(HF) theory, there exist some problems on the quantitative discussion of the energy. As a result, the difference might become fairly large between the considering two potential barriers. Therefore, the energy should be re-estimated using recent high level ab initio MO calculations. Furthermore, there has been no discussion about the rates of the competing reactions theoretically. This paper presents the theoretical rate constants for path (1) and (2) at a more sophisticated level and discusses the reaction dynamics for the decomposition of formic acid.

2 Methods of Calculation

Ab initio MO and the density functional theory(DFT) calculations were carried out with the GAUSSIAN98 [13] program packages. All geometries of the reactants, products, and transition states(TSs) were determined with analytically calculated energy gradients at the HF theory and the DFT using Becke's three-parameter non-local-exchange functional [14–16] and the non-local correlation functional of Lee, Yang and Parr [17](B3LYP) with Dunning's correlation consistent basis sets known as cc-pVDZ and cc-pVTZ [18]. Vibrational frequencies were calculated by using the analytical second derivatives at the B3LYP/cc-pVDZ and B3LYP/cc-pVTZ to

confirm the stationary structures and correct for the zero-point vibrational energy. Frequencies are scaled to 0.8929 times for the HF calculations and 0.9613 times for the B3LYP calculations [19]. These values were determined for the 6-31G(d) basis set, not cc-pVDZ and cc-pVTZ basis sets. This treatment was thought to be a proper approximation. For TSs, only one imaginary frequency was obtained.

The intrinsic reaction coordinate(IRC) calculations by Fukui [11] was followed from the TS toward both reactants and products. The normal vibrational analysis along the IRC was carried out by diagonalizing the Hessian matrices in the mass weighted coordinates after projecting out the component in the direction of the IRC. The reaction path Hamiltonian for a non-rotating polyatomic molecule, formulated by Miller et al. [20], is as follows:

$$H(p_s, s, \{P_k, Q_k\}, k = 1, \cdots, F-1) = \frac{\frac{1}{2}[p_s - \sum_{k,k'}^{F-1} Q_k P_{k'} B_{k,k'}(s)]^2}{[1 + \sum_{k=1}^{F-1} Q_k B_{k,F}(s)]^2} + \frac{1}{2}\sum_{k=1}^{F-1}(P_k^2 + \omega_k(s)^2 Q_k^2) + V_0(s), \qquad (3)$$

where s and p_s are the reaction coordinate(IRC, in this case) and its conjugate momentum, respectively, $V_0(s)$ is the potential energy along the IRC as a function of s, and Q_k and P_k are coordinates and momenta for vibrations perpendicular to the IRC, with frequencies $\omega_k(s)$. The curvature coupling element $B_{k,F}$ mixes the vibrational mode k with the reaction coordinate s, and the intermode Coriolis coupling element $B_{k,k'}$ mixes the vibrational mode k and k'. Here, all the force constants and coupling elements are truncated at the second order. The total curvature of the IRC $\kappa(s)$ is the magnitude of the $(F-1)$ dimensional vector made of $B_{k,F}$:

$$\kappa(s) = [\sum_{k=1}^{F-1} B_{k,F}(s)^2]^{1/2}. \qquad (4)$$

And we define root mean square I(s) of intermode coupling $B_{k,k'}$ as a physical quantity representing the total of intermode coupling:

$$I(s) = [\sum_{k<k'}^{F-1} B_{k,k'}(s)^2]^{1/2}. \qquad (5)$$

3 Results and discussion

Optimized structures of Z-formic acid, E-formic acid, and TS structures for path (1) and (2), which correspond to three-center and four-center TS, respectively, are shown in Fig. 1. It is noticed that the four-center TS is planar, while the three-center TS is not planar. Vibrational frequencies of these species multiplied by the scaling factor are shown in Table 1. In the following figures, each vibrational mode is numbered in order of vibrational frequencies of the reactant. Fig. 1 shows a schematic energy profile of formic acid system with zero-point energy corrections. Table 2 shows relative energies using various calculation levels of theory. The MP4/6-31G//HF/6-31G level (adopted in the study of ref. [5]) was confirmed to be a comparatively low computational level for the geometry optimization, because polarization functions are not included. One of the conclusions of Saito et al. [5] is that the difference of the rates between the two paths was attributable to the difference of the energy barriers. However, in the case of higher level ab initio calculations with added polarization functions for the geometry optimization such as MP4/cc-pVQZ//B3LYP/cc-pVTZ level, energy barriers of the two reaction paths become close to each other. Using these results, rate constants are estimated from the conventional transition state theory. Pre-exponential factors A(in s^{-1}) and activation energy E_a(in kcal mol^{-1}) are listed in Table 3. In the calculations, rate constants for the two reaction paths are mostly comparable. Thus, the experimental results which show a large difference between the two paths are not explained by the conventional transition state theory. Recently, we tried a shock tube experiment again in order to obtain the ratio of the product using a sensitive analyzer for produced CO and CO_2 [21]. According to this experiment, the ratio [CO]/[CO_2] was around forty, supporting our early work. Therefore, we need to get more detailed information about the potential energy surfaces of path (1) and (2) in order to solve this problem.

Vibrational frequencies of the reacting molecule along the IRC for the two paths are shown in Fig. 2(a) and (b). In these figures, although we performed high

level ab initio calculations, we have gotten a similar behavior to the early work by Yamashita et al [12]. As seen in Fig. 2, there appears a large difference in the change of the vibrational frequencies between the two paths. For path (1)(Fig. 2(a)), after the TS (near s=1), there is a large change in the CH stretching(mode 7), following occurrence of a large bending motion of H-O-H(mode 5), while the other modes change slightly over whole reaction path. On the other hand, for path (2)(Fig. 2(b)), there are some drastic changes of vibrational mode around the TS, for example, OH stretching(mode 8) and CH stretching(mode 7), whereas some vibrational modes such as CO stretching(mode 6), do not change so much, thus these modes do not contribute this path.

The behavior of couplings with the IRC are shown in Fig. 3(a) and (b). In Fig. 3(a), the curvature of path (1) is small over the whole reaction path, except for a sharp peak near s=1 corresponding to the change of the CH stretching of the reactant to the OH stretching of the product(H_2O). On the other hand, in the case of path (2)(Fig. 3(b)), the situation is different from path (1). There is a large hill of the curvature ($B_{k,F}$) at the entrance region of path (2). Near the TS, the curvature becomes small, and there is again a large peak near s=0.5, then the curvature decreases in the exit region. Thus, at the initial stage of the reaction and after the TS(near s=1), energy transfer between vibrational modes and the IRC happens.

The behavior of intermode couplings are shown in Fig. 4(a) and (b). In these figures, only significant intermode couplings are shown. The magnitude of intermode couplings are larger for path (1) than for path (2), indicating that energy transfer between vibrational modes are larger along path (1) than along of path (2).

In Table 3, calculated rate constants by using the conventional transition state theory are also shown. The competing reaction rates are $k_1 = 4.71 \times 10^5 s^{-1}$ and $k_2 = 1.93 \times 10^5 s^{-1}$ at 1500K. The ratio $k_1/k_2 = 2.44$. According to the experiment, the ratio is about forty at the same temperature. This large discrepancy of the ratio between the experiment and the theoretical calculation might be explained by the

large difference of the couplings ($B_{k,F}$'s and $B_{k,k'}$'s) between path (1) and (2).

If the curvature is large, the energy transfer between the IRC and related vibrational modes becomes large, i.e., the internal energy of the IRC mode diffuse easily to the vibrational modes. Here, we will consider the relationship between the intramolecuar energy transfer and the reaction rate. Chemical reaction is accelerated by transferring energies to the IRC mode. If the curvature is small, energy transfer between the IRC and some vibrational modes is difficult. In this case, near the TS the IRC mode is in a state likely as adiabatic. On the other hand, if the curvature is large, energy transfer to the vibrational modes is easy, and this will result in a decrease of the reaction rate. Thus the rate constant becomes low. Here, the IRC mode is likely as non-adiabatic. From above discussion, the curvature of reaction coordinate is important to examine the reaction rate as same as to examine the internal energy transfer. This is a new interpretation for the relation between the curvature of reaction coordinate and the reaction rate.

Actually, this proposal must be supported by dynamical calculations. Classical trajectory calculations were performed for formic acid using semi-empirical MO theory [22]. In these calculations, for path (1), if mode specific excitation along the reaction coordinate is performed, many reactive trajectories occurred. On the other hand, for path (2), there were no reactive trajectories for the same excitation energy of path (1). These results are consistent with our prediction from the IRC calculations.

4 Summary

In this paper, important information of the dynamics near the IRC are discussed for the two reaction paths of formic acid. Energy barriers for the two reaction paths are almost same and pre-exponential factors are also resemble, however, rate constants expected from the conventional transition state theory can't explain a large difference in the rate constants between path (1) and (2). The dynamics near

the IRC is thought to differ in the two paths. From the analysis of the curvature along the IRC, in path (1), it is expected that there are fast processes which are not expected from the conventional transition state theory. This explanation must be supported by some dynamical studies for the unimolecular decomposition of formic acid. In the near future, our classical trajectory calculations for the formic acid decomposition will be reported.

5 Acknowledgement

This study is supported by a Grant-in-Aid on Research for the Future "Photoscience" (JSPS-RFTF-98P01202) from Japan Society for the Promotion of Science. The authors thank the Institute for Numerical Simulations and Applied Mathematics at Hiroshima University, for the use of COMPAQ Personal Workstation 433au.

References

[1] P.G.Blake and S. C.Hinshelwood, *Proc. R. Soc. London Ser.A*, 255(1960) 444.

[2] P.G.Blake, H.H.Davies, and G.Jackson, *J. Chem. Soc.*, (1971) 1923.

[3] R.Corkum, C.Willis, and R.A.Back, *Chem. Phys.*, 24(1977) 13.

[4] D.S.Hsu, W.M.Shaub, M.Blackbrun, and M.C.Lin, in 'The Ninteenth International Symposium on Combustion', The Combustion Institute, Pittsburgh, 1983, p 89.

[5] K. Saito, T. Kakumoto, H. Kuroda, S. Torii, and A. Imamura, *J. Chem. Phys.*, 80(1984) 4989.

[6] K. Saito, K. Shimofuji, K. Adachi, M. Watanabe, and A. Imamura, in 'National Symposium on Shock Wave Phenomena, Sep. 28-30', ISAS, Sagamihara, Japan, 1989, p 65.

[7] J.Lundell, M. Rasanen, and Z. Latajka, *J. Phys. Chem.*, 97(1993) 1152.

[8] Y.T.Chang, Y.Yamaguchi, W.H.Miller, and I. H.F.Schaefer, *J. Am. Chem. Soc.*, 109(1987) 1330.

[9] I.Yokoyama, Y.Miwa, and K.Machida, *J. Am. Chem. Soc.*, 113(1991) 6458.

[10] I.V.Tokmakov, C.-C.Hsu, L.V.Moskaleva, and M.C.Lin, *Mol. Phys.*, 92(1997) .

[11] K.Fukui, *J. Am. Chem. Soc.*, 74(1970) 4161.

[12] K.Yamashita and T.Yamabe, *Int. J. Quantum Chem. Symp.*, 17(1983) 177.

[13] M. J. Frisch, G. W. Trucks, H. B. Schlegel, G. E. Scuseria, M. A. Robb, J. R. Cheeseman, V. G. Zakrzewski, J. A. Montgomery, J. R. E. Stratmann, J. C. Burant, S. Dapprich, J. M. Millam, A. D. Daniels, K. N. Kudin, M. C. Strain, O. Farkas, J. Tomasi, V. Barone, M. Cossi, R. Cammi, B. Mennucci, C. Pomelli,

C. Adamo, S. Clifford, J. Ochterski, G. A. Petersson, P. Y. Ayala, Q. Cui, K. Morokuma, D. K. Malick, A. D. Rabuck, K. Raghavachari, J. B. Foresman, J. Cioslowski, J. V. Ortiz, B. B. Stefanov, G. Liu, A. Liashenko, P. Piskorz, I. Komaromi, R. Gomperts, R. L. Martin, D. J. Fox, T. Keith, M. A. Al-Laham, C. Y. Peng, A. Nanayakkara, C. Gonzalez, M. Challacombe, P. M. W. Gill, B. Johnson, W. Chen, M. W. Wang., J. L. Andres, C. Gonzalez, M. Head-Gordon, E. S. Replogle, and J. A. Pople. Gaussian 98, revision a.4.

[14] A.D.Becke, *J. Chem. Phys.*, 96(1992) 2155.

[15] A.D.Becke, *J. Chem. Phys.*, 97(1992) 9173.

[16] A.D.Becke, *J. Chem. Phys.*, 98(1993) 564.

[17] C.Lee, W.Yang, and R.G.Parr, *Phys. Rev. B*, 37(1988) 785.

[18] J. T.H.Dunning, *J. Chem. Phys.*, 90(1989) 1007.

[19] J.B.Foresman and A.Frisch, 'Exploring Chemistry with Electronic Structure Methods, Second Ed.', Gaussian Inc., 1993.

[20] W.H.Miller, N.C.Handy, and J.E.Adams, *J. Chem. Phys.*, 72(1980) 99.

[21] K.Saito. unpublished results.

[22] O.Takahashi and K.Saito. unpublished results.

Table 1: Vibrational frequencies(in cm^{-1}) for the transition state of path (1) and (2) at the B3LYP/cc-pVTZ level of theory. Scaling factor(0.9613) have already multiplied for all vibrational modes.

species	ν_i / cm^{-1}
Z-HCOOH	605.8, 660.1, 1014.6, 1081.2, 1255.4, 1351.0, 1755.6, 2926.8, 3578.2
E-HCOOH	512.1, 636.4, 995.9, 1068.3, 1225.5, 1365.3, 1798.9, 2841.0, 3642.4
TS1	1560.9i, 309.4, 355.1, 562.2, 740.4, 1005.3, 1876.7, 2514.7, 3617.2
TS2	2132.8i, 592.7, 702.0, 838.9, 1012.7, 1288.2, 1666.4, 1960.2, 2031.1

Table 2: Relative energies(in kcal mol^{-1}) from zero point energy level of Z-HCOOH. Zero point energy correction is added for each case.

	Z-HCOOH	E-HCOOH	TS1[a]	TS2[a]	H_2O+CO	H_2+CO_2
MP4/6-31G//HF/6-31G	0.0	5.9	61.3	80.2	2.5	-12.8
MP4/6-31G(d,p)//HF/6-31G(d,p)	0.0	5.2	77.9	78.1	9.8	-4.1
MP4/cc-pVTZ//HF/cc-pVDZ	0.0	4.2	65.9	67.1	4.1	-7.9
MP4/cc-pVQZ//HF/cc-pVTZ	0.0	4.0	64.7	63.5	3.8	-7.9
MP4/cc-pVTZ//B3LYP/cc-pVDZ	0.0	4.2	64.5	66.5	4.3	-8.3
MP4/cc-pVQZ//B3LYP/cc-pVTZ	0.0	4.1	63.4	66.3	4.1	-8.0

[a] TS1 and TS2 mean transition state for path (1) and (2), respectively.

Table 3: Arrhenius parameters using the conventional transition state theory. Rate constants k at 1500K are also shown.

	path 1		
	A / s^{-1}	E_a / kcal mol^{-1}	k / s^{-1}
MP4/cc-pVTZ//HF/cc-pVDZ	7.46×10^{15}	64.0	
MP4/cc-pVQZ//HF/cc-pVTZ	8.26×10^{15}	62.9	
MP4/cc-pVTZ//B3LYP/cc-pVDZ	4.64×10^{14}	67.5	
MP4/cc-pVQZ//B3LYP/cc-pVTZ	5.27×10^{14}	62.1	4.71×10^5
exp[a]		53.0	
	path 2		
	A / s^{-1}	E_a / kcal mol^{-1}	k / s^{-1}
MP4/cc-pVTZ//HF/cc-pVDZ	1.26×10^{15}	59.2	
MP4/cc-pVQZ//HF/cc-pVTZ	8.86×10^{14}	55.9	
MP4/cc-pVTZ//B3LYP/cc-pVDZ	8.53×10^{13}	64.6	
MP4/cc-pVQZ//B3LYP/cc-pVTZ	8.18×10^{13}	59.2	1.93×10^5
exp[a]		72.5	

[a] This barrier heights are estimated from $E_{a,0}$ using the RRKM theory. See in reference [5].

Figure captions.

- Fig.1 Schematic energy profile of formic acid system with zero-point energy corrections. Energy value is MP4/cc-pVQZ//B3LYP/cc-pVTZ level.

- Fig.2 Vibrational frequencies along the IRC using B3LYP/cc-pVTZ. (a)path (1). (b)path (2).

- Fig.3 The IRC curvatures and coupling with the IRC along the IRC using B3LYP/cc-pVTZ. Each vibrational mode is numbered in small order of vibrational frequencies at the TS. (a)path (1). (b)path (2). For both figures, a thick solid line indicates curvature κ(s).

- Fig.4 Intermode couplings along the IRC using B3LYP/cc-pVTZ. Each vibrational mode is numbered in small order of vibrational frequencies at the TS. (a)path (1). (b)path (2). For both figures, a thick solid line indicates root mean square of intermode coupling I(s).

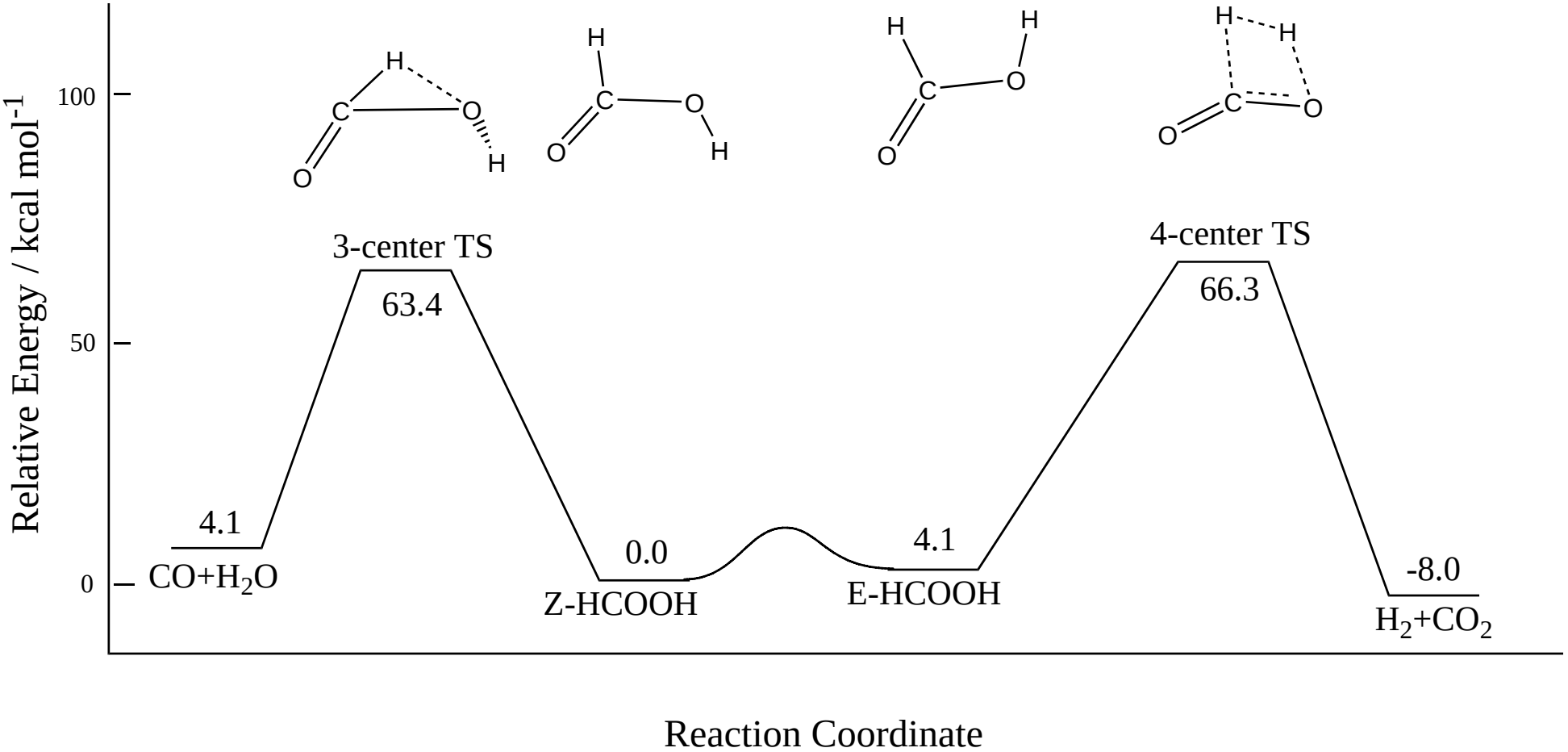
Relative Energy / kcal mol-1
100
50
0
3-center TS
63.4
4-center TS
66.3
4.1
CO+H2O
0.0
Z-HCOOH
4.1
E-HCOOH
-8.0
H2+CO2
Reaction Coordinate

fig.1

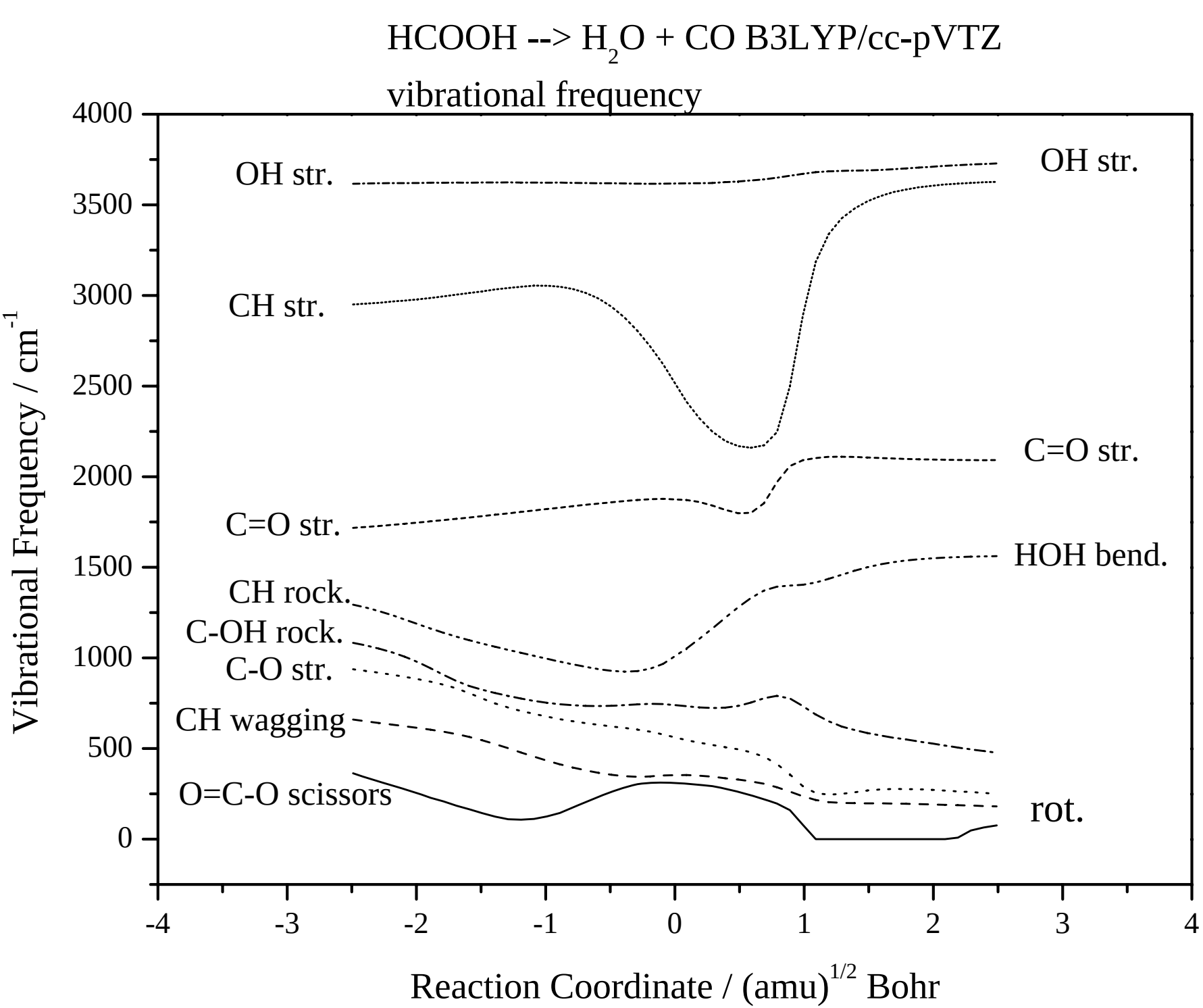
HCOOH --> H2O + CO B3LYP/cc-pVTZ
vibrational frequency
Vibrational Frequency / cm-1
4000
3500
3000
2500
2000
1500
1000
500
0
OH str.
CH str.
C=O str.
CH rock.
C-OH rock.
C-O str.
CH wagging
O=C-O scissors
OH str.
C=O str.
HOH bend.
rot.
-4
-3
-2
-1
0
1
2
3
4
Reaction Coordinate / (amu)1/2 Bohr

Fig.2(a)

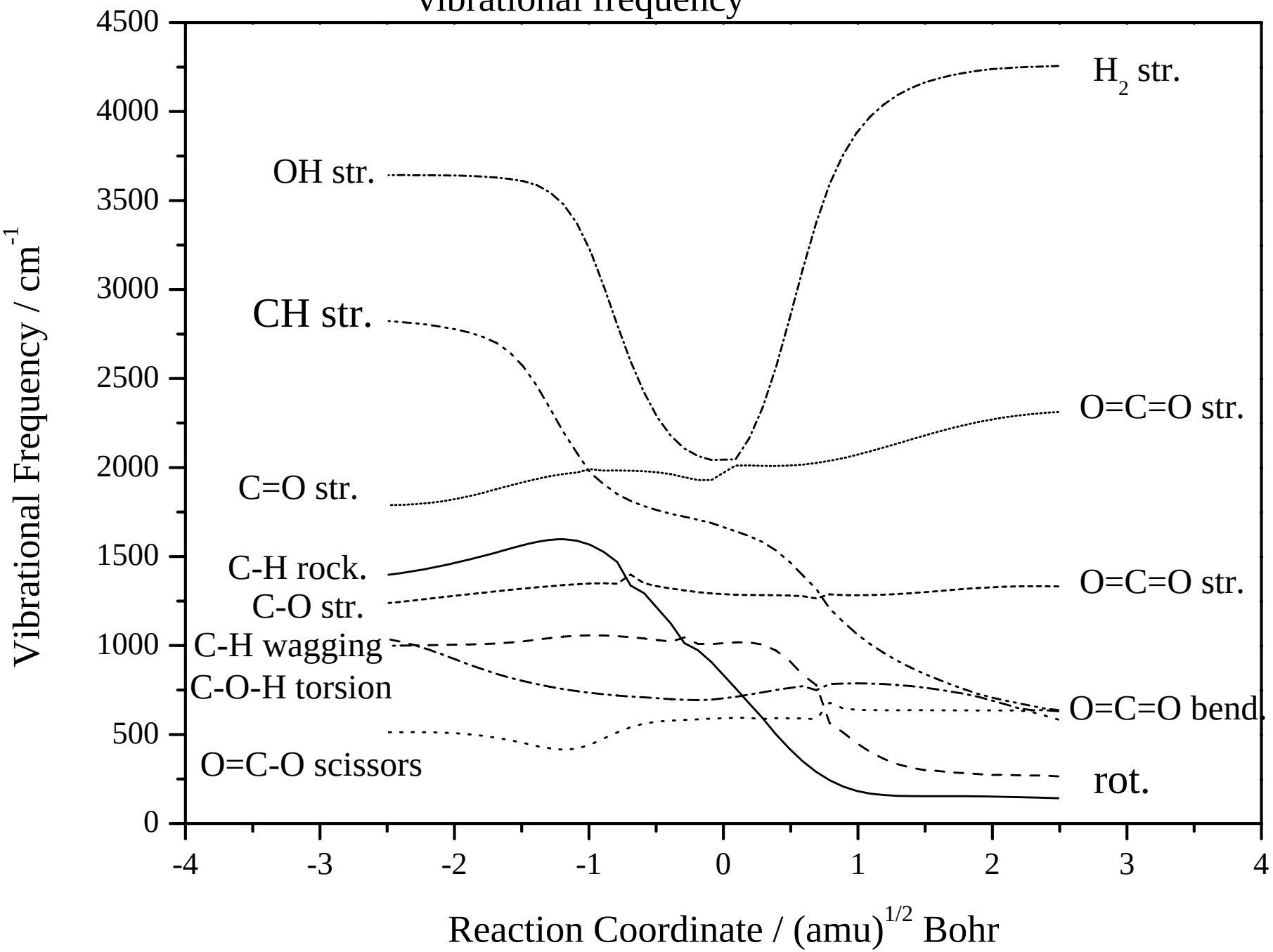
HCOOH --> H2 + CO2 B3LYP/cc-pVTZ
vibrational frequency
Vibrational Frequency / cm-1
Reaction Coordinate / (amu)1/2 Bohr
4500
4000
3500
3000
2500
2000
1500
1000
500
0
-4
-3
-2
-1
0
1
2
3
4
H2 str.
OH str.
CH str.
O=C=O str.
C=O str.
C-H rock.
O=C=O str.
C-O str.
C-H wagging
C-O-H torsion
O=C=O bend.
O=C-O scissors
rot.

Fig.2(b)

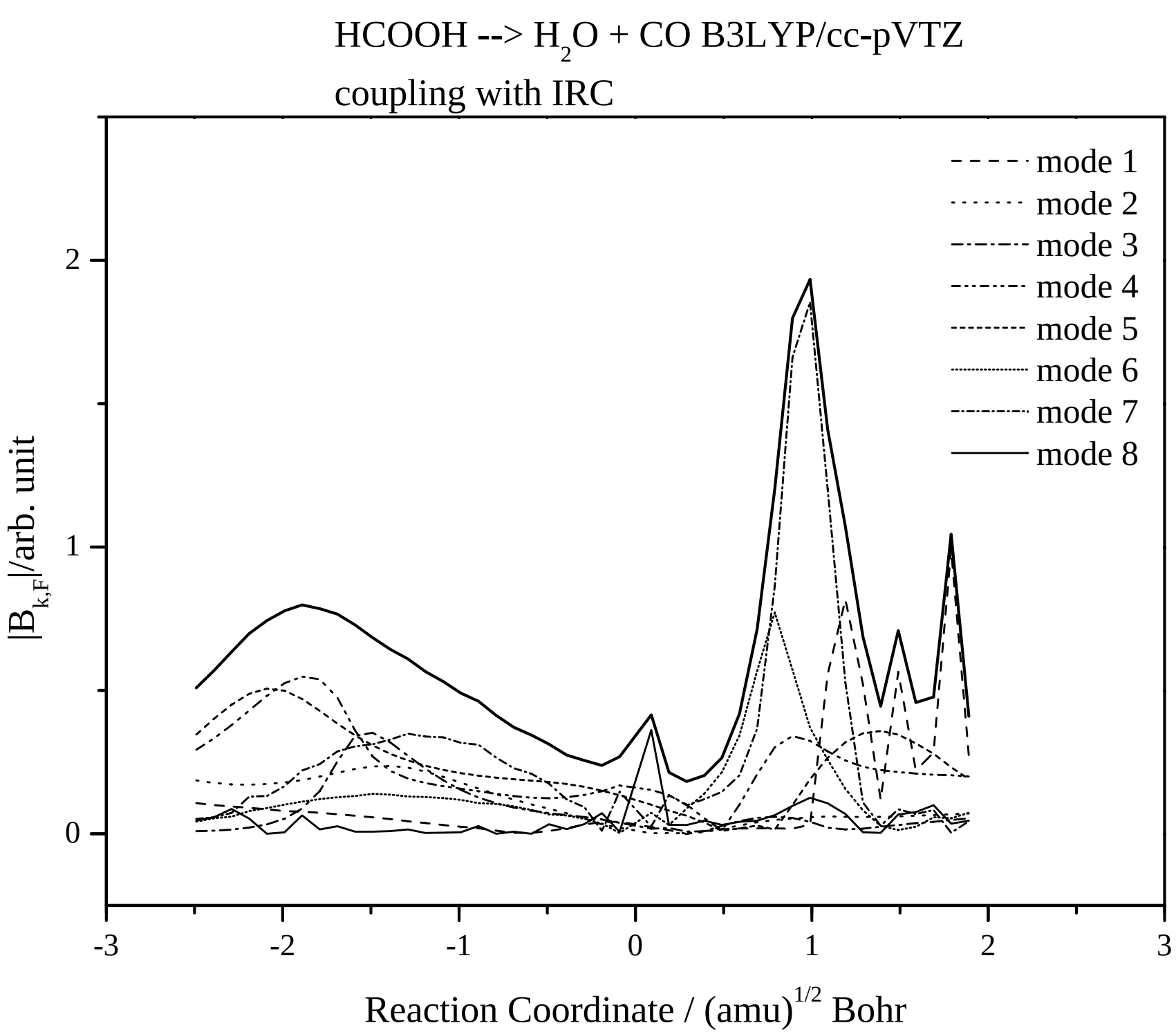
HCOOH --> H2O + CO B3LYP/cc-pVTZ
coupling with IRC
mode 1
mode 2
mode 3
mode 4
mode 5
mode 6
mode 7
mode 8
|Bk,F|/arb. unit
0
1
2
-3
-2
-1
0
1
2
3
Reaction Coordinate / (amu)1/2 Bohr

Fig.3(a)

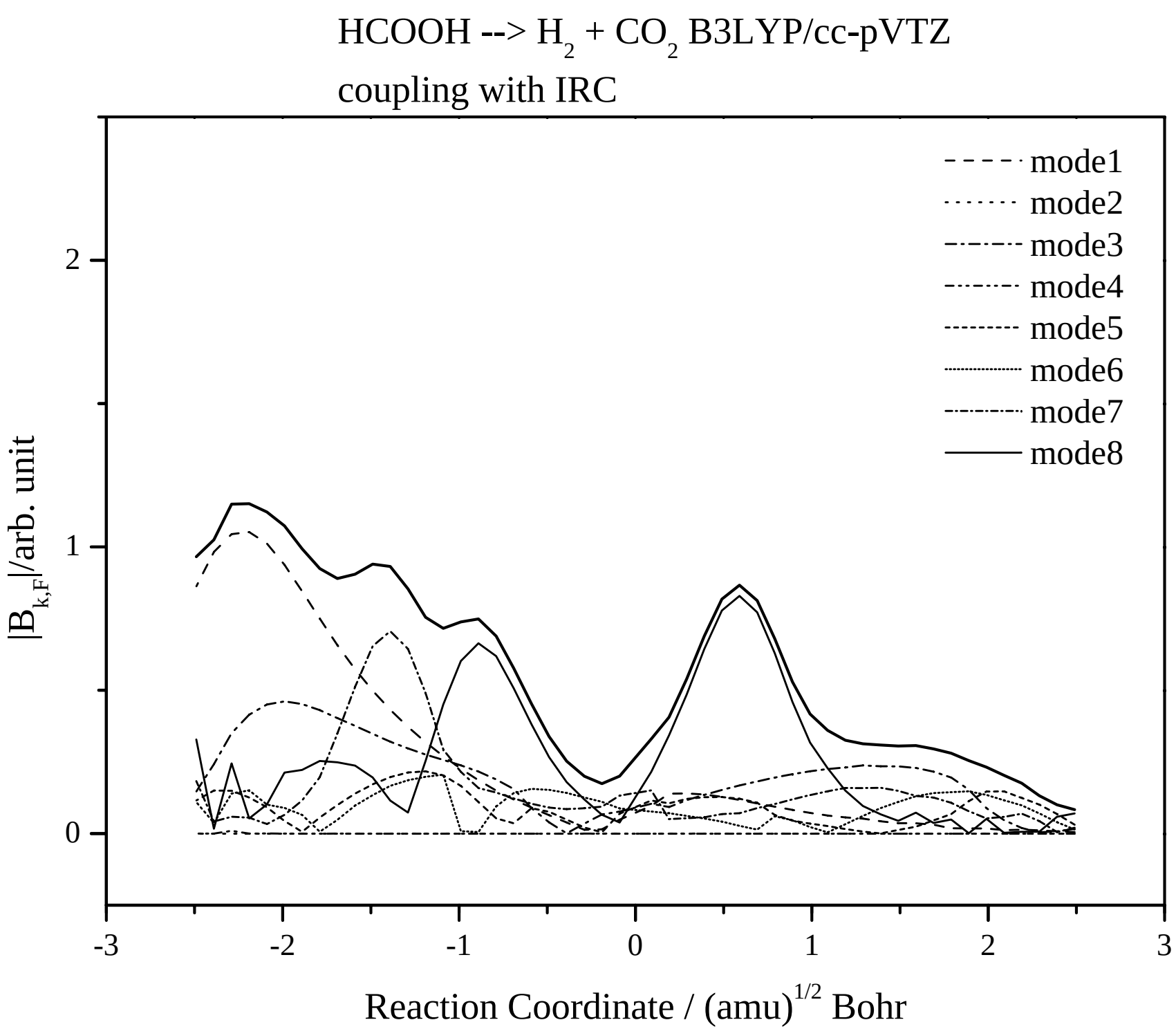
HCOOH --> H2 + CO2 B3LYP/cc-pVTZ
coupling with IRC
mode1
mode2
mode3
mode4
mode5
mode6
mode7
mode8
|Bk,F|/arb. unit
0
1
2
-3
-2
-1
0
1
2
3
Reaction Coordinate / (amu)1/2 Bohr

Fig.3(b)

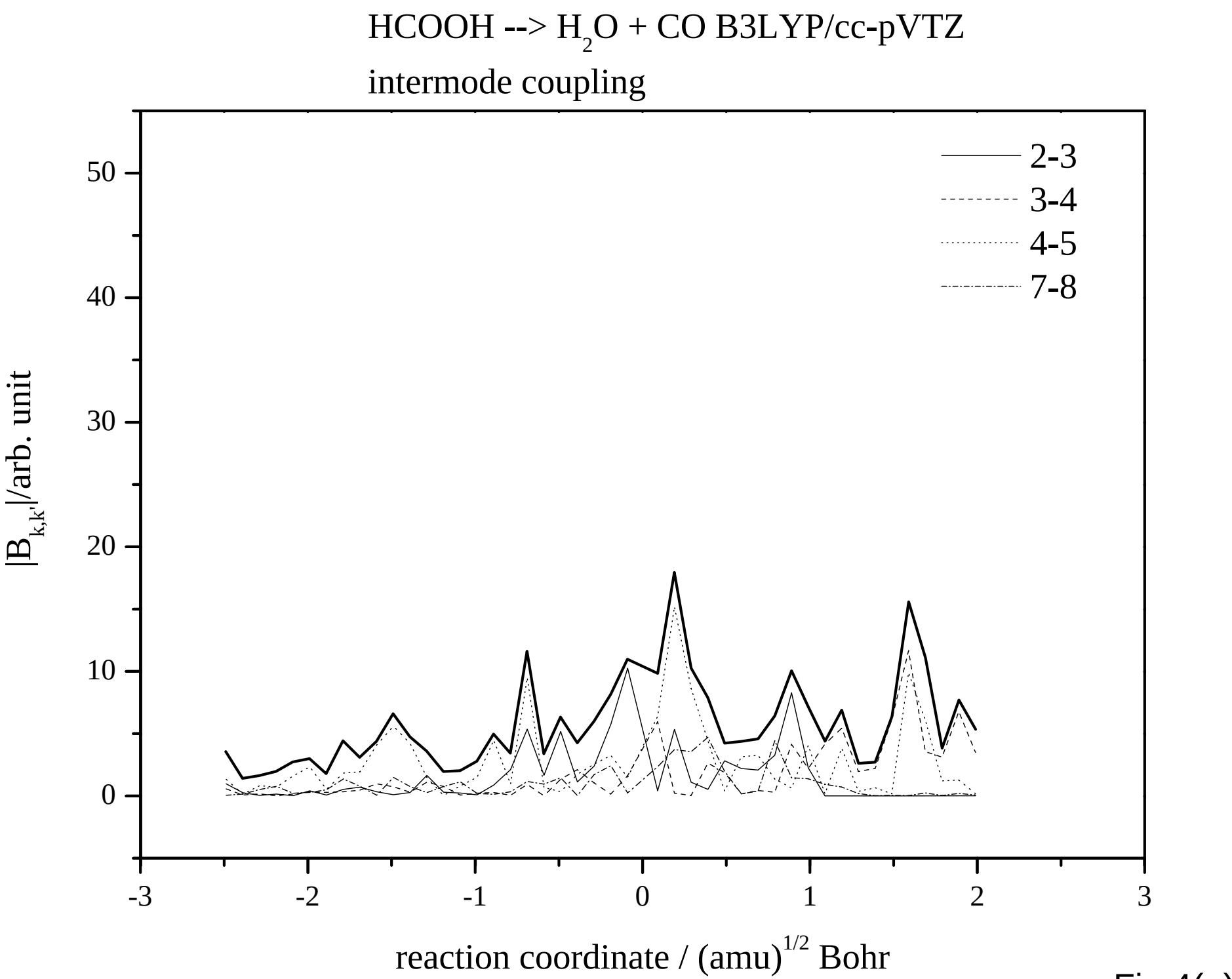
HCOOH --> H2O + CO B3LYP/cc-pVTZ
intermode coupling
2-3
3-4
4-5
7-8
|Bk,k'|/arb. unit
reaction coordinate / (amu)1/2 Bohr
50
40
30
20
10
0
-3
-2
-1
0
1
2
3

Fig.4(a)

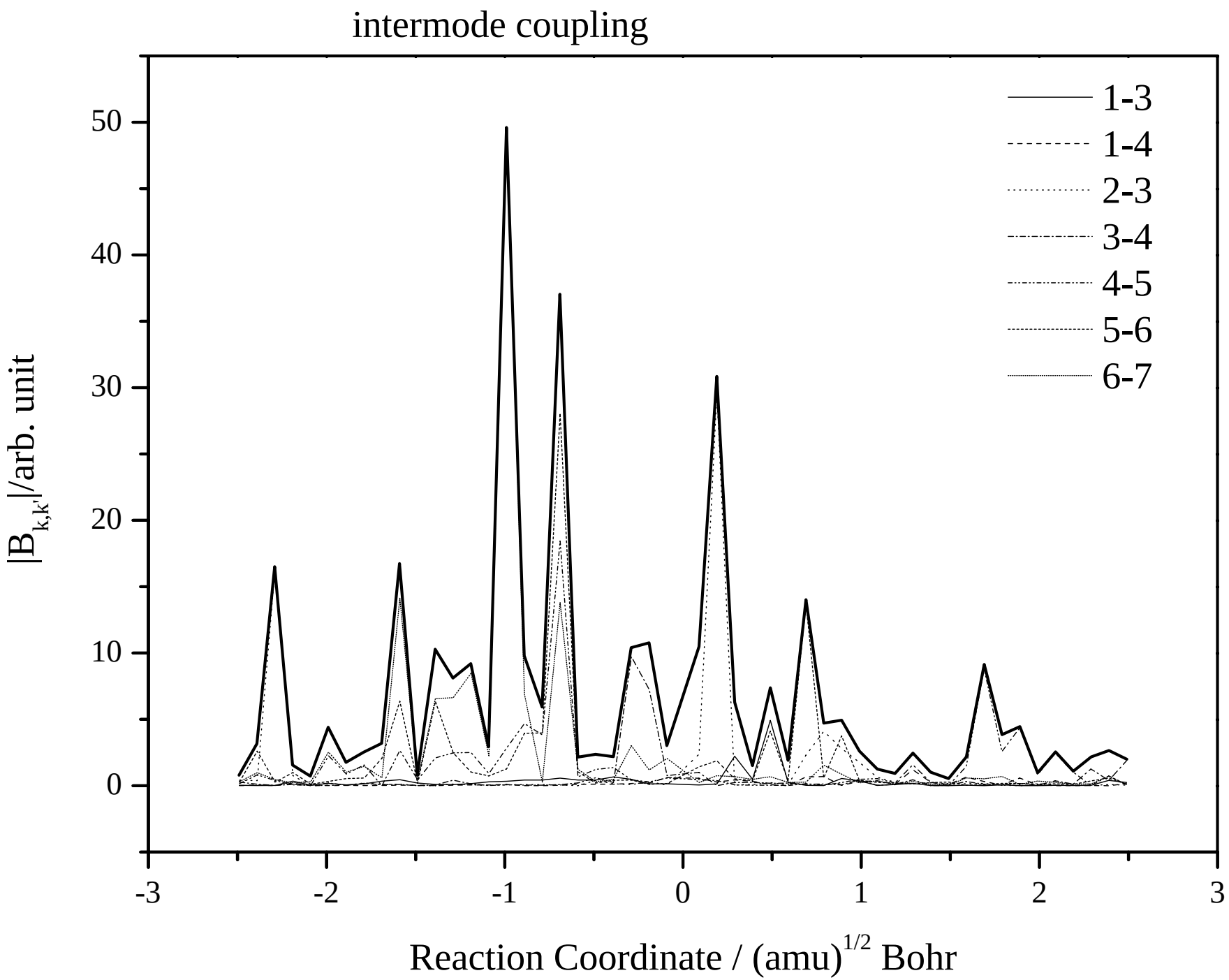
HCOOH --> H_2 + CO_2 B3LYP/cc-pVTZ
intermode coupling
1-3
1-4
2-3
3-4
4-5
5-6
6-7
50
40
30
20
10
0
-3
-2
-1
0
1
2
3
$|B_{k,k'}|$/arb. unit
Reaction Coordinate / $(amu)^{1/2}$ Bohr

Fig.4(b)

Erratum to "A Theoretical Study of the Bifurcation Reaction of Formic Acid: Dynamics around the Intrinsic Reaction Coordinate"; J. Mol Struct. (Theochem) 545 (2001) 197-205

Osamu TAKAHASHI, Kuniharu ITOH, Akio KAWANO and Ko SAITO*

Department of Chemistry, Graduate School of Science, Hiroshima University, 1-3-1, Kagamiyama, Higashi-Hiroshima 739-8526, JPN

It is regretted that a number of errors occurred in the above referenced article. The corrected extracts are now reprinted below.

Page 199, column 2, line 17 should read:

"[23]. According to this experiment, the ratio [CO]/"

Page 200, column 2, the third paragraph should read:

"The behavior of intermode couplings are shown in Fig. 4(a) and (b). In these figures, only significant intermode couplings are shown. The magnitude of intermode couplings are larger for path (2) than for path (1), indicating that energy transfer between vibrational modes are larger along path (2) than along of path (1)."

Page 205, column 2, reference 23 should be added:

"[23] K.Saito, T.Shiose, O.Takahashi, K.Okada, M.Nakamura, to be published."